/ The University of Electro-Communications

Practical Model Construction and Stable Control of an Unmanned Aerial Vehicle With a Parafoil-Type Wing

Practical Model Construction and Stable Control of an Unmanned Aerial Vehicle with a Parafoil Type Wing

Motoyasu Tanaka, *Member, IEEE*, Kazuo Tanaka, *Fellow, IEEE,* and Hua O. Wang, *Senior Member, IEEE*

Abstract—This paper presents a framework for practical model construction and stable altitude control of an unmanned aerial vehicle with a parafoil type wing (UAV-PW). To design a stable controller, we first construct a dynamical longitudinal model of the UAV-PW. Since there exist no aerodynamics data of the parafoil shape in our UAV-PW, aerodynamics coefficients balanced at the trimmed equilibrium are employed. The model accuracy is investigated by comparing the model outputs with the real test flight experimental data. Next, stable controller design conditions for the UAV-PW model with uncertainties are derived in terms of linear matrix inequalities (LMIs). By solving the LMI conditions, we design a stable controller that asymptotically stabilizes the UAV-PW model with the uncertainties on a considered operation domain. The experimental results demonstrate the viability of the model construction and the stable altitude control.

Index Terms—linear matrix inequality, model construction, stable control, unmanned aerial vehicle with parafoil type wing.

I. INTRODUCTION

A large number of studies on unmanned aerial vehicles (UAVs) development, navigation and control [1]-[10] have been reported in recent years. Most of the UAV studies discussed in the literature deal with fixed wing type [2], [3], [4], rotary wing type aerial vehicles [1], [5], [6] or their applications [7]-[10]. In comparison with those fixed/rotary UAV studies, a few studies on UAVs with soft and flexible wings such as parafoils have been presented for the past several years. For instance, only modeling/simulation studies [11] and human manual control studies [12], [13] were attempted for an unmanned aerial vehicle with a parafoil type wing (UAV-PW). The works [11] on the detailed modeling of a UAV-PW focused on constructing simulator dynamics and analyzing its dynamics rather than designing a stable controller. Although the paper [14] deals with linearized control for the dynamical model constructed by them, only simulation results have been reported. Modeling and control of parafoil-payload systems were reported in [15], [16]. However, the techniques in [15], [16] are unavailable for our UAV-PW since the parafoil structure of the UAV-PW is different from that

of the parafoil-payload systems. The difference will be briefly mentioned in Section II. As an advantage for the above existing studies, the approach in this paper will be carried out under the following policies:(i) experimental validation rather than simulation validation, (ii) systematic model-based controller design rather than trial-and-error controller design. In UAV control, experimental validation is much more reliable and valuable than only simulation validation, even if simulation results work perfectly. In addition, in experiments, guarantee of the stability for flight control systems is expected to avoid any flight troubles and to reduce the effort of trial-and-error controller gain tuning, etc. As an systematic model-based controller design, adaptive control based on neural networks (NNs) has been utilized in robotics control, e.g. [17]-[20]. Although they are interesting approaches for nonlinear systems from the theoretical points of view, most of these studies have provided only simulation results. The study [19], [20] has dealt with manipulator control experiments. The first priority of real UAV control is to secure real flight safety and to consider hardware/software implementation in *real* flight experiments and/or environments. In fact, it is reported in [21] that adaptive control schemes have some difficulties in hardware/software implementation and/or real flight safety even if adaptive control schemes work perfectly in simulations. Thus, to the best of our knowledge, there have been almost no NN-based adaptive control studies dealing with small-scale fixed wings and/or UAVs-PW in real flight experiments and/or environments. Although a few studies have dealt with experiments, only specific environments (indoor, etc.) have been considered. In this paper, we provide a practical model construction and stable control for real UAVs-PW and show its utility in real flight experiments and/or environments. There have been no UAVs-PW studies that have achieved the two points simultaneously, i.e., stable nonlinear controller design, validation by real flight experiments, for UAVs-PW.

The paper [22] presented an autonomous flight control result in experiments. However, it does not guarantee the stability of the control system that is one of the most important issues in UAV control. To the best of our knowledge, there are no UAVs-PW studies that provide both any controller designs guaranteeing the stability of considered control systems and any successful flight control experimental results, excepting the recent work [23]. The work [23] presented both a controller design guaranteeing the stability of a UAV-PW control system and flight control experimental results in practice. However, the dynamics constructed in [23] was not a precise model since

M. Tanaka, K. Tanaka are with Department of Mechanical and Intelligent Systems Engineering , The University of Electro-Communications, Tokyo, 182-8585 Japan (email:mtanaka@uec.ac.jp;ktanaka@mce.uec.ac.jp).

H. O. Wang is with Department of Mechanical Engineering, Boston University, Boston, MA, 02215, USA (email:wangh@bu.edu).

the parafoil aerodynamics were replaced with the NACA2412 data for a (rigid) fixed wing. In fact, it should be noted that the NACA2412 wing shape for a rigid fixed wing is not similar to the soft and flexible parafoil shape. Therefore, it is easily guessed that the model is not accurate. In fact, they did not evaluate the model accuracy and did not discuss the stability for the model uncertainty caused by the model error. This paper presents a more practical model construction, in particular, by considering the trimmed equilibrium of the parafoil type wing. In addition, we evaluate the model accuracy and show that the model outputs agree well with flight experimental data. However, the constructed model is still not a perfect model. Therefore, we introduce model uncertainties that include unprecise parameters and/or unmodeled dynamics. This paper also realizes robust control for the UAV-PW model with the uncertainties. Thus, by proposing a practical framework of modeling and control for the UAVs-PW, the purpose of this paper is to realize simultaneously both of two things:controller designs guaranteeing the stability of the UAV-PW control system, and successful real flight control experiments in practice. There are no UAVs-PW studies that provide simultaneously both of them. In other words, this paper aims at achieving the above two things rather than comparing the design method proposed in this paper with the existing methods. The comparison itself is out of scope of this paper.

In this paper, a dynamical longitudinal model of a UAV-PW is constructed to design a stable controller. A main problem in the UAV-PW model construction is that there exist no aerodynamics data of the parafoil type wing since parafoils are made by light, soft and flexible materials. Hence, we employ aerodynamics coefficients balanced at the trimmed equilibrium. The model accuracy is investigated by comparing the model outputs with the real test flight experimental data. The model outputs agree with the experimental data of real flights. However, it is practically useful to consider the model error caused by the aerodynamics coefficients and some simplifications. Hence, this paper will consider model uncertainties in the stable controller design of Section III. Stable controller design conditions for the UAV-PW model with the uncertainties are derived in terms of linear matrix inequalities (LMIs). Hence, by solving the LMI conditions, we design a stable controller that asymptotically stabilizes the UAV-PW model with the uncertainties on a considered operation domain. The experimental results demonstrate the viability of the model construction and the stable altitude control.

It is assumed that all the matrices and vectors in this paper have appropriate dimensions. $P \succ 0$ $(P \succeq 0)$ means that P is a positive definite matrix (positive semi-definite matrix).

II. UAV-PW MODEL WITH THREE DEGREE OF FREEDOM

Fig. 1 shows the photo of UAV-PW during flight. The body size $(L \times W \times H)$ of the UAV-PW is $390[mm] \times 54[mm] \times 285[mm]$. The UAV-PW has a DC motor (connected to the propeller) that generates the thrust force and a parafoil (parachute) that generates the lift force. Fig. 2 shows the UAV-PW body (excepting the parafoil) with the control unit and the

direction bar, and principles of left-turn and right-turn. All the lines (cables) from the front and rear edges of the parafoil are connected to both ends of the direction bar. By rotating the direction bar via a servo motor, the parafoil is tilted without changing its shape. By changing the directions of the lift/drag force vectors according to the rotation of the direction bar, the UAV-PW can change the direction. We note again that the parafoil structure of our UAV-PW is different from that of the parafoil-payload systems in [15], [16]. The important point for its mechanical structure is that the UAV-PW never have the left and right brakes (it also has no the speed bar). Just one servo motor is used for controlling the direction bar in the UAV-PW.

Fig. 3 shows the UAV-PW coordinate system and some important variables to describe the motion of flight, where a three-degree of freedom (3-DOF) motion model (x, z and θ) is considered on x-z coordinate system. Due to the peculiar structure of the UAV-PW, the pivot point of the pitching motion, the so-called pitch center [24], [25] considering the apparent mass effect, is located around the parafoil. Table I lists the variables and parameters in the UAV-PW model.

Fig. 1. Photo of UAV-PW during flight.

TABLE I
LIST OF VARIABLES AND PARAMETERS IN UAV-PW MODEL.

$x, \dot{x}$	x position [m], its velocity [m/s] in world coordinate system
$z, \dot{z}$	z positions [m], its velocity [m/s] in world coordinate system
v_c	parafoil velocity vectors
v_p	body velocity vectors
u	thrust force [N]
L	lift force [N]
D	drag force [N]
θ	angle difference between body and parafoil [rad.]
α	attack of angle [rad.]
m	mass of body 1.3 [kg]
I_y	moment of inertia of body [$kg \cdot m^2$]
S	area of parafoil 0.97 [m^2]
l	distance between body center and parafoil center 1.2 [m]
ρ	air density 1.2250 [kg/m^3]
C_L	lift coefficient
C_D	drag coefficient
g	acceleration of gravity [m/s^2]

Let us consider the parafoil velocity $v_c(t)$ and the body velocity $v_p(t)$. Clearly, $v_c(t) \simeq v_p(t)$, in particular, $v_c(t) = v_p(t)$ for the trimmed equilibrium around the steady flight condition. Hence, taking the reasonable assumption $v_c(t) = v_p(t) \equiv v(t)$ and $|v_c(t)|^2 = |v_p(t)|^2 = \dot{x}^2(t) + \dot{z}^2(t)$, the 3DOF
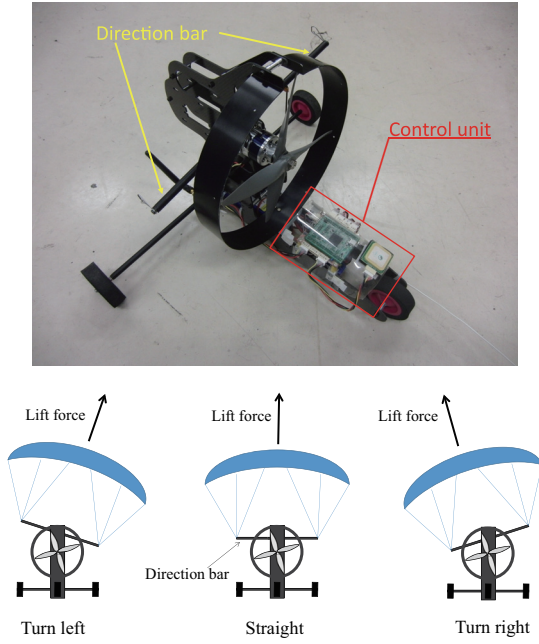
Fig. 2. Control unit and direction bar in UAV-PW excepting parafoil (upper photo) and principles of left-turn and right-turn (lower).
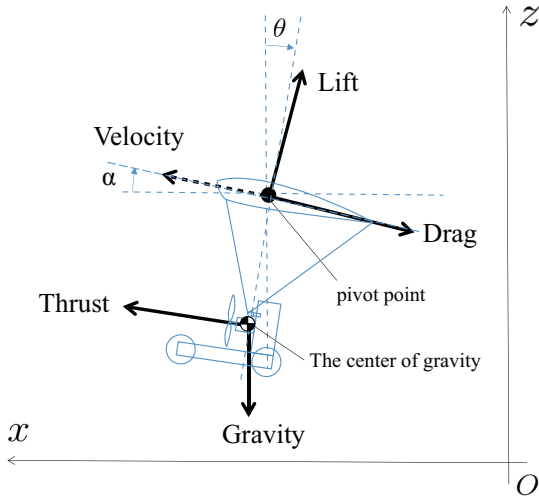

Fig. 3. UAV-PW coordinate system and some important variables.

UAV-PW model is described as

$$m\ddot{x}(t) = u(t)\cos\theta(t) - D_x(t) - L_x(t), \quad (1)$$
$$m\ddot{z}(t) = u(t)\sin\theta(t) - D_z(t) + L_z(t) - mg, \quad (2)$$
$$I_y\ddot{\theta}(t) = u(t)l - mgl\sin\theta(t), \quad (3)$$

where

$$L_x(t) = \frac{1}{2}\rho\{\dot{x}^2(t) + \dot{z}^2(t)\}C_L(\alpha(t))S\sin\alpha(t),$$
$$L_z(t) = \frac{1}{2}\rho\{\dot{x}^2(t) + \dot{z}^2(t)\}C_L(\alpha(t))S\cos\alpha(t),$$
$$D_x(t) = \frac{1}{2}\rho\{\dot{x}^2(t) + \dot{z}^2(t)\}C_D(\alpha(t))S\cos\alpha(t),$$
$$D_z(t) = \frac{1}{2}\rho\{\dot{x}^2(t) + \dot{z}^2(t)\}C_D(\alpha(t))S\sin\alpha(t).$$

$u(t)$ is the thrust force ([N]) generated by the DC motor. By considering the equilibrium condition of forces and moments (see Fig. 3), the model is constructed based on the above fact that the pivot point of the pitching motion is located around the parafoil. The real control input to the UAV-PW is the throttle position (from $0[\%]$ to $100[\%]$) of the DC motor. The relation between the thrust force ([N]) and the throttle position ([%]) is investigated throughout a preliminary experiment. Once a thrust force is calculated from a designed controller, it can be transformed to the corresponding throttle position using the investigated relation. $L_x(t)$ and $L_z(t)$ are the $x(t)$ and $z(t)$ axes components of the lift force vector, respectively. $D_x(t)$ and $D_z(t)$ are the $x(t)$ and $z(t)$ axes components of the drag force vector, respectively.

Consider the altitude error $e(t)$ defined as $e(t) = z(t) - z_r$, where z_r denotes the constant target altitude [m]. Note that $\dot{e}(t) = \dot{z}(t)$ and $\ddot{e}(t) = \ddot{z}(t)$. In addition, by assuming the trimmed equilibrium (the steady flight condition), we arrive at the dynamics

$$m\ddot{e}(t) = u(t)\sin\theta^s + \frac{1}{2}\rho C_M^s(V^s)^2 + \frac{1}{2}\rho C_M^s\dot{e}^2(t) - mg, \quad (4)$$

where $V^s = \dot{x}^s$ and $C_M^s = C_L^s S\cos\alpha^s - C_D^s S\sin\alpha^s$. By the assumption, the variables with the superscript 's' become constants obtained around the trimmed equilibrium. V^s means the speed of steady-state flight, i.e., the speed of keeping constant altitudes. All the values are determined from the trimmed equilibrium flight data or wind tunnel experimental data in the test flight experiments, where $C_L^s = 0.479$, $C_D^s = 0.146$, $V^s = 6.4$ [m/s], $\alpha^s = 0$ and $\theta^s = 8.44$ [deg.]. The steady-state thrust force is 3.7 [N] that corresponds to the steady-state throttle position $65[\%]$.

We evaluate the accuracy of the model (4) constructed at the considered trimmed equilibrium. First, we rewrite (4) as

$$\ddot{e}(t) = \frac{\sin\theta^s}{m}u(t) + \frac{1}{2m}\rho C_M^s(V^s)^2 + \frac{1}{2m}\rho C_M^s\dot{e}^2(t) - g.$$

We evaluate the model accuracy by calculating the mean absolute error between the model output and the test flight experimental data. Table II shows the evaluation results of one-step ahead prediction errors for four different experimental data sets measured at the different days, where MAE, SD and N denotes the mean absolute error, standard deviation and the number of data to calculate the MAE and SD, respectively. Fig. 4 shows the evaluation result for the first worst case (Data 2). Fig. 5 shows the evaluation result for the second worst case (Data 4). Even for the two worst cases (Data 2 and Data 4), the MAEs are small.

TABLE II
MODEL EVALUATION.

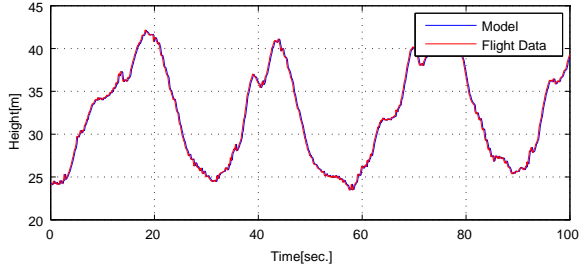| Data	MAE [m]	SD	N
Data 1	0.1750	0.2376	1000
Data 2	0.3016	0.3786	1000
Data 3	0.1711	0.2253	1000
Data 4	0.1988	0.2571	1000
Ave.	0.2116	0.2747	-

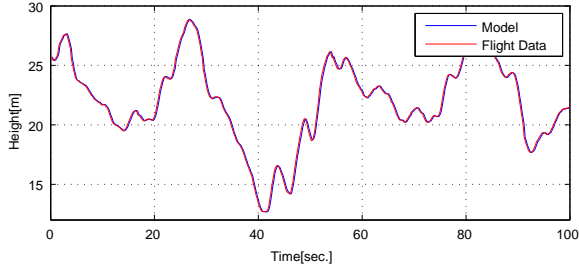Fig. 4. Evaluation result for the first worst case (Data 2).

Fig. 5. Evaluation result for the second worst case (Data 4).

It is known that the one-step ahead prediction error becomes very small, particularly, in case the sampling of the data is fast. Conversely, multiple-steps ($\ell > 1$) ahead prediction is a more stringent test of model accuracy than the one-step ahead prediction. The multiple-steps ahead prediction is a successive one-step ahead prediction, where, in the case of ℓ-steps ahead prediction for $t \in [t_s \ t_s + \ell \cdot \Delta t]$, the integrated value for the $\ddot{e}(t)$ in each consecutive step are utilized as the value of $\dot{e}(t)$ for the next step of prediction, where t_s denotes the starting time in the ℓ-steps ahead prediction and Δt denotes the sampling period of the flight experimental data. Only the input $u(t)$ and the initial values of $e(t_s)$ and $\dot{e}(t_s)$ are utilized as the DC motor torques and the initial altitude position and velocity errors measured in the experimental data. Fig. 6 shows the calculation procedure of MAE in the ℓ-steps ahead prediction, where $\Delta t = 0.1[sec.]$. If a large ℓ-step ahead prediction is carried out, the reliability of the model accuracy is higher. A larger ℓ-steps ahead prediction could be a better evaluation. However, in practice, the larger ℓ-steps ahead prediction might lead to diverging outputs. In this paper, we select $\ell = 10, 50, 100$ that correspond to one-second (ten samples) ahead prediction, five-second (fifty samples) ahead prediction, ten-second (one hundred samples) ahead prediction, respectively. In our case, it is reasonable to consider the case of $\ell \leq 100$ since the steady speed at the considered trimmed equilibrium is $V^s = 6.4$ [m/s], and this means that the model error for every flight (horizontal) distance 64 [m] is considered, i.e., a sufficient flight (horizontal) distance to evaluate the altitude model error. The MAEs in the ℓ-steps ahead prediction errors of the model output for the first worst case (Data 2) are calculated to evaluate the model accuracy. The results are obtained as 0.9519, 1.7798 and 2.2150 for $\ell = 10$, $\ell = 50$ and $\ell = 100$, respectively. Fig. 7 shows

the ℓ-steps ahead prediction results for $\ell = 10$, $\ell = 50$ and $\ell = 100$. Even in the $\ell = 100$ case for the first worst case (Data 2), the model with the trimmed parameters is reasonably useful for controller design purposes since the result shows that the model output has only 2.2 [m] error during every flight (horizontal) distance 64 [m].
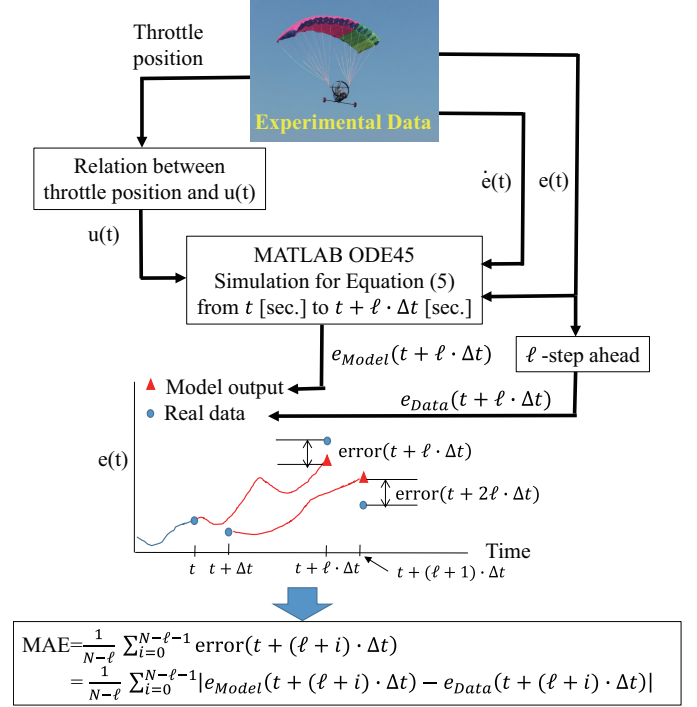
Fig. 6. Calculation procedure of MAE in ℓ-steps ahead prediction.

Thus, the UAV-PW model outputs agree well with the flight data. However, it is still not a perfect model. Therefore, we will introduce model uncertainties that include unprecise parameters and/or unmodeled dynamics in the stable controller design of Section III.

III. STABLE CONTROLLER DESIGN

Section III presents a stable controller design based on the model constructed in Section II.

Recall the model

$$\ddot{e}(t) = \frac{\sin \theta^s}{m} u(t) + \frac{1}{2m} \rho C_M^s (V^s)^2 + \frac{1}{2m} \rho C_M^s \dot{e}^2(t) - g.$$

For the model, we introduce model uncertainties that include unprecise parameters and/or unmodeled dynamics in the stable controller design.

$$\begin{aligned}
\ddot{e}(t) &= a_1(1 + \Delta_1(t))u(t) + a_2(1 + \Delta_2(t))(V^s)^2 \\
&\quad + a_2(1 + \Delta_2(t))\dot{e}^2(t) - g.
\end{aligned} \tag{5}$$

where

$$a_1 = \frac{\sin \theta^s}{m}, \ a_2 = \frac{1}{2m} \rho C_M^s.$$

In the model construction, we introduce model uncertainties as $a_1(1 + \Delta_1(t))$ and $a_2(1 + \Delta_2(t))$ instead of a_1 and a_2, respectively, where $||\Delta_1(t)|| \leq \frac{1}{\gamma_1}$ and $||\Delta_2(t)|| \leq \frac{1}{\gamma_2}$ for
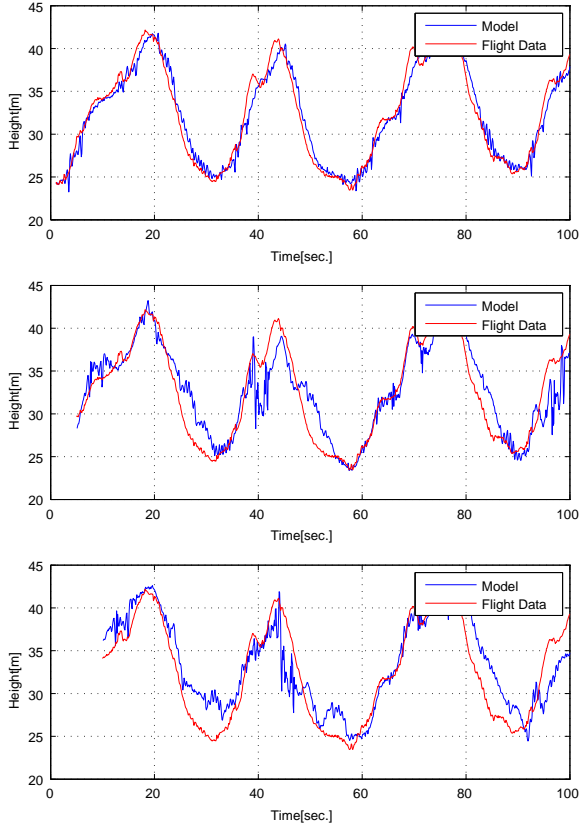
Fig. 7. ℓ-steps ahead prediction results for the first worst case (Data 2) (upper:$\ell = 10$, middle:$\ell = 50$, lower:$\ell = 100$).

all t. γ_1 and γ_2 are positive values. If we set $\frac{1}{\gamma_1} = 0.1$ and $\frac{1}{\gamma_2} = 0.05$, the setting represents the model within $\pm 10\%$ change of the parameter a_1 and $\pm 5\%$ change of the parameter a_2. In this paper, $\gamma_1 = \gamma_2 = 20$.

Consider the following controller consisting of a term and a PD controller.

$$u(t) = u_N^s + (f_1 e(t) + f_2 \dot{e}(t)), \qquad (6)$$

where f_1 and f_2 are feedback gains in the PD controller. We will derive a set of stable controller design conditions to determine the feedback gains later. The term u_N^s is determined by measuring the trimmed input to keep the same altitude through flight experiments. In other words, from the practical flight control points of view, it can be considered to satisfy the equality,

$$a_1(1 + \Delta_1(t))u_N^s + a_2(1 + \Delta_2(t))(V^s)^2 - g = 0. \qquad (7)$$

It should be noted from (5) that $\ddot{e}(t) = 0$ when $u(t) = u_N$ and $\dot{e}(t) = 0$. In fact, we confirm in flight experiments that the UAV-PW flies a constant altitude ($\dot{e}(t) = 0$, i.e., it keeps the same altitude) when $u = u_N$. The term u_N^s realizes the gravity compensation and cancellation of a part of the nonlinearities around the considered trimmed equilibrium.

The overall control system consisting of (5) and (6) is

described as

$$\begin{aligned} \ddot{e}(t) &= a_1(1 + \Delta_1(t))(f_1 e(t) + f_2 \dot{e}(t)) \\ &\quad + a_2(1 + \Delta_2(t))\dot{e}^2(t). \end{aligned} \qquad (8)$$

The dynamics is still nonlinear due to existing the term $\dot{e}^2(t)$. Now, to determine the feedback gains f_1 and f_2 satisfying the stability of the feedback system, let us introduce a polytypic model representation.

$$\begin{aligned} \ddot{e}(t) &= a_1(1 + \Delta_1(t))f_1 e(t) \\ &\quad + \{a_1(1 + \Delta_1(t))f_2 + a_2(1 + \Delta_2(t))\dot{e}(t)\}\dot{e}(t) \\ &= a_1(1 + \Delta_1(t))f_1 e(t) \\ &\quad + \{a_1(1 + \Delta_1(t))f_2 + a_2(1 + \Delta_2(t))p(t)\}\dot{e}(t) \end{aligned} \qquad (9)$$

where $-d < p(t)(= \dot{e}(t)) < d$. In this paper, d is set to 3. Since the maximum absolute value of the velocity $\dot{z}(t)$ of the UAV-PW is $2 \sim 2.5$ [m/s], the range $-3 < \dot{e}(t) < 3$ is enough to guarantee the stability of the overall system in practice. If the UAV-PW flies over the above range, the controller might be unable to work well. However, due to the actuator (thrust force generation) limitation, the upward speed is less than 2.5 [m/s]. On the other hand, the downward speed is also kept about 2.5 [m/s] (due to slowly down by the parachute effect) even with zero thrust force during control. Thus, the considered range is enough to guarantee the stability of the overall system in practice. Finally, (9) is represented as

$$\begin{aligned} \dot{e}(t) &= \sum_{i=1}^{2} \eta_i(p(t))(\boldsymbol{A}_i + \boldsymbol{D}_A \Delta_2(t)\boldsymbol{E}_{Ai} \\ &\quad + (\boldsymbol{B} + \boldsymbol{D}_B \Delta_1(t)\boldsymbol{E}_B)\boldsymbol{F})\boldsymbol{e}(t), \\ &= \sum_{i=1}^{2} \eta_i(p(t))(\boldsymbol{A}_i + \boldsymbol{B}\boldsymbol{F} + \boldsymbol{Z}\boldsymbol{H}_i(t))\boldsymbol{e}(t), \quad (10) \end{aligned}$$

where $\boldsymbol{e}(t) = [e(t) \ \dot{e}(t)]^T$ and $\boldsymbol{F} = [f_1 \ f_2]$,

$$\boldsymbol{A}_1 = \begin{bmatrix} 0 & 1 \\ 0 & -a_2 d \end{bmatrix}, \boldsymbol{A}_2 = \begin{bmatrix} 0 & 1 \\ 0 & a_2 d \end{bmatrix}, \boldsymbol{B} = \begin{bmatrix} 0 \\ a_1 \end{bmatrix},$$

$$\boldsymbol{D}_A = \begin{bmatrix} 0 \\ a_2 \end{bmatrix}, \boldsymbol{D}_B = \begin{bmatrix} 0 \\ a_1 \end{bmatrix},$$

$$\boldsymbol{E}_{A1} = \begin{bmatrix} 0 & -d \end{bmatrix}, \ \boldsymbol{E}_{A2} = \begin{bmatrix} 0 & d \end{bmatrix}, \boldsymbol{E}_B = 1,$$

$$\boldsymbol{Z} = [\boldsymbol{D}_A \ \boldsymbol{D}_B], \boldsymbol{H}_i(t) = \begin{bmatrix} \Delta_2(t) & 0 \\ 0 & \Delta_1(t) \end{bmatrix} \begin{bmatrix} \boldsymbol{E}_{Ai} \\ \boldsymbol{E}_B \boldsymbol{F} \end{bmatrix},$$

$$\eta_1(p(t)) = \frac{d - p(t)}{2d}, \eta_2(p(t)) = \frac{d + p(t)}{2d}.$$

Note that

$$\eta_1(p(t)) + \eta_2(p(t)) = 1$$

for all $p(t)$, and $\eta_i(p(t)) > 0$ ($i = 1, 2$) under the assumption

$$-d < p(t)(= \dot{e}(t)) < d.$$

To determine the feedback gains $\boldsymbol{F}$, we derive a set of LMI conditions satisfying the stability of (10) via a common Lyapunov function approach [26], [27]. Let us consider a candidate Lyapunov function $V(\boldsymbol{e}(t)) = \boldsymbol{e}^T(t)\boldsymbol{P}\boldsymbol{e}(t)$, where $\boldsymbol{P}$ is a positive definite matrix. It is clear that $V(\boldsymbol{e}(t)) > 0$ at $\boldsymbol{e}(t) \neq \boldsymbol{0}$ and $V(\boldsymbol{e}(t))$ is radially unbounded.

The stability condition of the control system is derived by taking time derivative of $V(e(t)) = e^T(t)Pe(t)$ along the trajectory of (10).

$$
\begin{aligned}
\dot{V}(e(t)) &= \dot{e}^T(t)Pe(t) + e^T(t)P\dot{e}(t) \\
&= \sum_{i=1}^{r} \eta_i(p(t))e^T(t)\{\mathcal{L}\{PA_i + PBF\} \\
&\quad + H_i^T(t)Z^T P + PZH_i(t)\}e(t) \quad (11)
\end{aligned}
$$

where $\mathcal{L}\{P\} = P^T + P$. Note that

$$
-\left(Z^T P - H_i(t)\right)^T \left(Z^T P - H_i(t)\right) \preceq 0. \quad (12)
$$

From this property, (11) satisfies

$$
\begin{aligned}
\dot{V}(e(t)) &\leq \sum_{i=1}^{r} \eta_i(p(t))e^T(t)\{\mathcal{L}\{PA_i + PBF\} \\
&\quad + PZZ^T P + H_i^T(t)H_i(t)\}e(t) \quad (13)
\end{aligned}
$$

Clearly if (14) is satisfied, $\dot{V}(e) < 0$ at $e \neq 0$ holds.

$$
\mathcal{L}\{PA_i + PBF\} + PZZ^T P + H_i^T(t)H_i(t) \prec 0 \quad (14)
$$

The inequality (14) is still a non-convex condition with the feedback gain matrix F and the Lyapunov function matrix P. To obtain a convex condition, by multiplying (14) on the left and right by $X = P^{-1}$, we have

$$
\mathcal{L}\{A_i X + BM\} + ZZ^T + XH_i^T(t)H_i(t)X \prec 0. \quad (15)
$$

where $M = FX$. Since

$$
XH_i^T(t)H_i(t)X \preceq
\begin{bmatrix} XE_{Ai}^T & M^T E_B^T \end{bmatrix}
\begin{bmatrix} \frac{1}{\gamma_2^2}I & 0 \\ 0 & \frac{1}{\gamma_1^2}I \end{bmatrix}
\begin{bmatrix} E_{Ai}X \\ E_B M \end{bmatrix}, \quad (16)
$$

we have

$$
\mathcal{L}\{A_i X + BM\} + ZZ^T
+ \begin{bmatrix} XE_{Ai}^T & M^T E_B^T \end{bmatrix}
\begin{bmatrix} \frac{1}{\gamma_2^2}I & 0 \\ 0 & \frac{1}{\gamma_1^2}I \end{bmatrix}
\begin{bmatrix} E_{Ai}X \\ E_B M \end{bmatrix} \prec 0. \quad (17)
$$

By applying the well-known Schur complement [28] (see Appendix) to (17), we arrive at the following design conditions (18) and (19) to be asymptotically stable for (10) on the domain $-3 < \dot{e}(t) < 3$. Note that the considered domain is sufficient to guarantee the asymptotical stability in practice since the maximum absolute value of the velocity $\dot{z}(t)$ of our UAV-PW is $2 \sim 2.5$ [m/s].

The equilibrium of the system (10) is asymptotically stable on the considered domain if there exist a positive definite matrix X and a matrix M such that

$$
X \succ 0, \quad (18)
$$

$$
\begin{bmatrix}
\Omega_i & XE_{Ai}^T & M^T E_B^T \\
E_{Ai}X & -\gamma_2^2 I & 0 \\
E_B M & 0 & -\gamma_1^2 I
\end{bmatrix} \prec 0, \ i = 1, 2, \quad (19)
$$

where $X = P^{-1}$ and $M = FX$,

$$
\Omega_i = \mathcal{L}\{A_i X + BM\} + D_A D_A^T + D_B D_B^T. \quad (20)
$$

Thus, by solving the above LMI conditions (18) and (19), a stable feedback gain is obtained as $F = MX^{-1}$ from the solutions X and M. Since the inequalities (18) and (19) are LMIs (with respect to X and M), the LMIs can be numerically solved or determined that no solution exists by an LMI solver like the MATLAB® Robust Control Toolbox. The feedback gain satisfying the LMIs is obtained as $F = [-0.64476 \ -3.2839]$.

IV. CONTROL EXPERIMENT

Fig. 8 shows the system configuration for automatic flight control. The DC motor and the servo motor in the UAV-PW are for controlling the propeller and the direction bar, respectively. The control unit consists of a CPU board (Renesas Electronics Corporation, MH8SX1655), a GPS sensor (Fastrax Oy, UP500) and a microSD card unit. The sampling rate of the GPS sensor is 10 [Hz]. The battery on the UAV-PW is a 4000 [mA] LiPo battery (11.1 [V], 310 [g]). The UAV-PW with the battery can approximately fly around $30 \sim 35$ minutes. To control the DC motor, a speed controller is also installed on the body. The flight data obtained from the GPS are transmitted by the wireless module. The wireless camera is used to carry out aerial shooting tasks from the air. Visual information gathered from the wireless camera is received by the wireless camera receiver. The wireless module and camera are not used to directly control the UAV-PW.

Based on the altitude error, the UAV-PW is stabilized at the target altitude by controlling the DC motor. The UAV-PW flight information (the current position from the GPS sensor, the current velocity, time, the DC motor inputs, the servo motor inputs and flag for automatic/manual control mode, etc.) are recorded to the microSD card. The real time monitoring for the UAV-PW flight information is also realized through the wireless communication module. The control unit realizes the switching of the automatic flight control/manual flight control by the signal from the operator on the ground and saves the flag time chart for automatic/manual control mode.

The control experiments have been performed at an Taiki Japan Aerospace Exploration Agency (JAXA) Aerospace Research Field in Taiki, Hokkaido, Japan. The take-off and landing are controlled by operators in the control experiments. The direction is also controlled by operators.

Fig. 9 shows an altitude control experimental result of 3D plots and 2D plots (altitude vs. time), where the blue and red lines in the 2D plot denote the control result and target altitude, respectively. The target altitude is 60 [m], where the UAV-PW is controlled along the runway at the aerospace research field. The control result shows that the controller (6) stabilizes the UAV-PW. Thus, the designed controller works well even in the flight experiment.

To evaluate the control performance, we carry out control experiments in different four days. The results are summarize in Table III, where the MAEs and the SDs in the steady states are shown. The MAE is very small even for the worst result (Day II). Figs. 10 and 11 present the control results for the first and second worst results (Day II and Day IV), respectively. Fig. 12 shows the altitude error, the thrust force and velocity
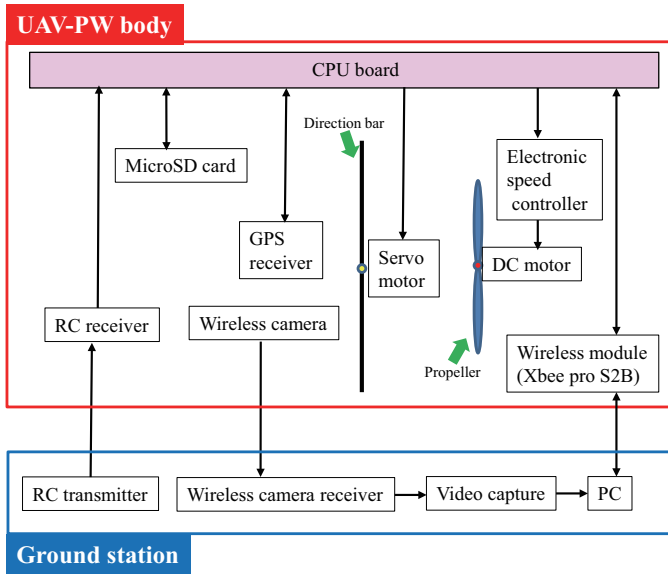
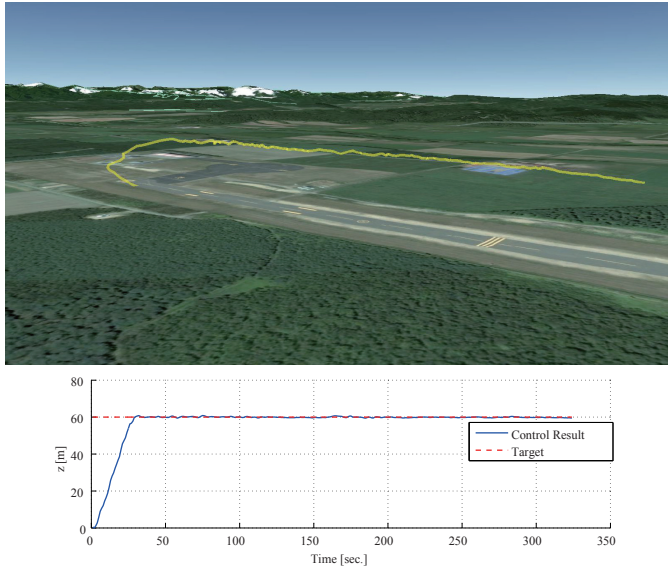Fig. 8. System configuration.

Fig. 9. Altitude control result (3-dimensional plot (upper) and 2-dimensional plot (lower)).

for the first worst result (Day II). It can be found from these figures that the designed controller stabilizes the UAV-PW well even in the worst results. These experimental results in Section IV demonstrate that the UAV-PW is stably controlled by the designed controller.

V. Conclusion

This paper has presented a framework for practical model construction and stable altitude control of a UAV-PW. To design a stable controller, we have first constructed a dynamical longitudinal model of the UAV-PW. Since there exist no aerodynamics data of the parafoil shape in our UAV-PW, aerodynamics coefficients balanced at the trimmed equilibrium have been employed. The model accuracy has been investi-

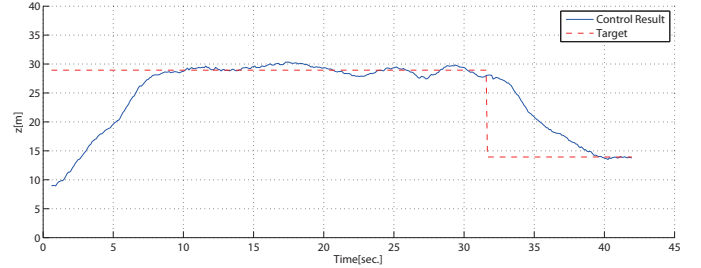| Day	MAE [m]	SD
Day I	0.3478	0.0389
Day II	0.4746	0.2368
Day III	0.3907	0.0927
Day IV	0.4519	0.0551
Ave.	0.4163	0.1059

Fig. 10. Control result for the first worst result (Day II).

gated by comparing the model outputs with the real test flight experimental data. Next, stable controller design conditions for the UAV-PW model with uncertainties have been derived in terms of LMIs. By solving the LMI conditions, we have designed a stable controller that asymptotically stabilizes the UAV-PW model with the uncertainties on a considered operation domain. The experimental results have demonstrated the viability of the model construction and the stable altitude control. In this paper, we have not considered input constraint [26], [29] and optimality [5], [27]. Our future work is to consider them in the UAV-PW controller design. Also it would be interesting to apply other nonlinear control techniques, e.g., [28], [30], [31], to the UAV-PW.

APPENDIX
SCHUR COMPLEMENT

Consider the real symmetric matrix described by

$$P = \begin{bmatrix} P_{11} & P_{12} \\ P_{12} & P_{22} \end{bmatrix}. \tag{21}$$

then, the following statements are equivalent [28].

1) $P \succ 0$
2) $P_{22} \succ 0$ and $P_{11} - P_{12}P_{22}^{-1}P_{12}^T \succ 0$
3) $P_{11} \succ 0$ and $P_{22} - P_{12}^T P_{11}^{-1} P_{12} \succ 0$

ACKNOWLEDGMENT

REFERENCES

[1] M. Sugeno, et al., "Fuzzy hierarchical control of an unmanned helicopter," Proceeding of 5th IFSA Congress, Seoul, July 1993, pp.179-182.
[2] D. J. Pack, et al., "Cooperative control of UAVs for localization of intermittently emitting mobile targets," IEEE Transactions on Systems, Man and Cybernetics PART B, Vol.39, No.4, pp.959-970, August 2009.
[3] P. Iscold, et al., "Development of a hand-launched small UAV for ground reconnaissance," IEEE Transactions on Aerospace and Electronic Systems, Vol.46, No.1, pp.335-348, January 2010.
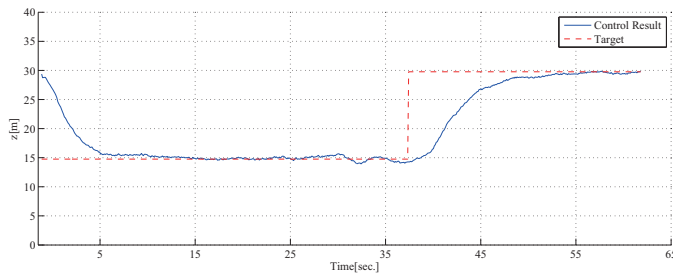
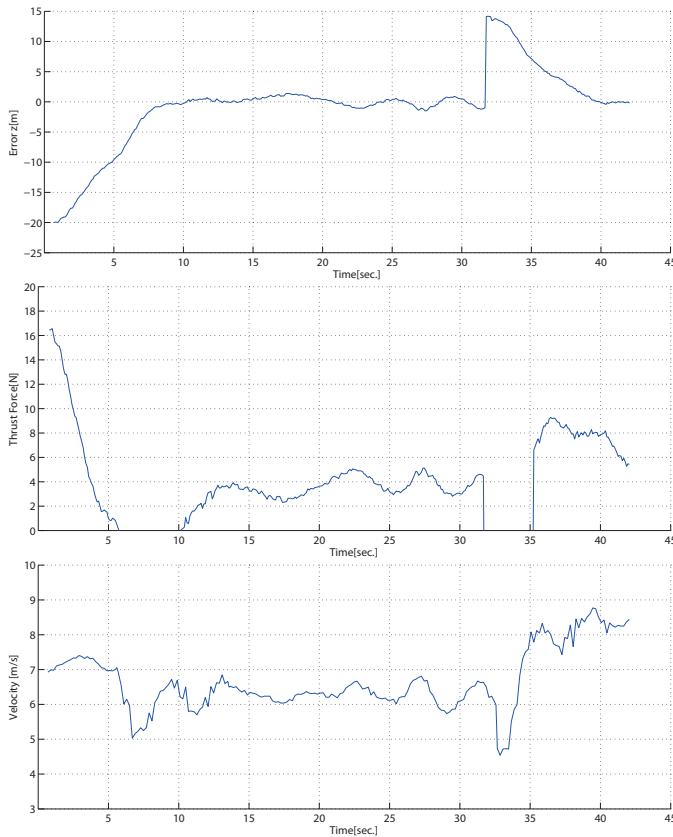Fig. 11. Control result for the second worst result (Day IV).

Fig. 12. Altitude error, thrust force and velocity in the first worst control result (Day II).

[4] J. Tisdale, et al., "Autonomous UAV path planning and estimation," IEEE Robotics & Automation Magazine, Vol.16, No.2, pp.35-42, June 2009.

[5] K. Tanaka, H. Ohtake, M. Tanaka and H. O. Wang, "Wireless vision-based stabilization of indoor micro helicopter," IEEE/ASME Transactions on Mechatronics, Vol.17, No.3, pp.519-524, June 2012.

[6] S. Saripalli, et al., "Visually guided landing of an unmanned aerial vehicle," IEEE Transactions on Robotics and Automation, Vol.19, No.3, pp.371-380, June 2003.

[7] C. C. Murray and W. Park., "Incorporating Human Factor Considerations in Unmanned Aerial Vehicle Routing," IEEE Transactions on Systems, Man, and Cybernetcs:Systems, Vol.43, No.4, pp.860-874, July 2013.

[8] Y. Fu, M. Ding, C. Zhou and H. Hu, "Route Planning for Unmanned Aerial Vehicle (UAV) on the Sea Using Hybrid Differential Evolution and Quantum-Behaved Particle Swarm Optimization," IEEE Transactions on Systems, Man, and Cybernetcs:Systems, Vol.43, No.6, pp.1451-1465, Nov. 2013.

[9] C. Teuliere, E. Marchand, and L. Eck, "3-D Model-Based Tracking for UAV Indoor Localization," IEEE Transactions on Cybernetcs, Vol.45, No.5, pp.869-879, May 2015.

[10] R. Mitchell and I. Chen "Adaptive Intrusion Detection of Malicious Unmanned Air Vehicles Using Behavior Rule Specifications," IEEE Transactions on Systems, Man, and Cybernetcs:Systems, Vol.44, No.5, pp.593-604, May 2014.

[11] Y. Ochi and M. Watanabe, "Modelling and simulation of the dynamics of a powered paraglider," Proceedings of the Institution of Mechanical Engineers, Part G: Journal of Aerospace Engineering, Vol.225, No.4, pp.373-386, April 2011.

[12] P. Proctor, "Production nears for low-cost parachute-based UAV," Aviation Week & Space Technology. Vol.145, No.20, pp.53-54, Nov. 1996.

[13] T. Huba, I. Pestun, and M. Huba, "Learning by pleasure - powered paraglider and other UAVs control," 2011 14th International Conference on Interactive Collaborative Learning (ICL), Piestany, Slovakia, Sept. 2011, pp.548-552.

[14] Y. Ochi, H. Kondo and M.Watanabe, "Linear dynamics and PID flight control of a powered paraglider," AIAA Guidance, Navigation, and Control Conference, Chicago, Illinois, August 2009, AIAA 2009-6318.

[15] N. Slegers, "Effects of canopy-payload relative motion on control of autonomous parafoils," Journal of guidance, control, and dynamics, vol. 33, No.1, pp.116-125, Jan-Feb. 2010.

[16] N. Slegers and M. Costello, "Model Predictive Control of a Parafoil and Payload System," Journal of guidance, control, and dynamics, Vol. 28, No. 4, pp.816-821, July-August 2005.

[17] W. He, Y. Dong and C. Sun "Adaptive Neural Impedance Control of a Robotic Manipulator With Input Saturation," IEEE Transactions on Systems, Man, and Cybernetics:Systems, Vol.46, No.3, pp.334-344, March 2016.

[18] L. Jin, S. Li, H. M. La and X. Luo, "Manipulability Optimization of Redundant Manipulators Using Dynamic Neural Networks ," IEEE Transactions on Industrial Electronics, Vol.64, No.6, pp.4710-4720, Feb. 2017

[19] W. He, Y. Ouyang and J. Hong, "Vibration Control of a Flexible Robotic Manipulator in the Presence of Input Deadzone," IEEE Transactions on Industrial Informatics, Vol.13, No.1, pp.48-59, Feb. 2017.

[20] A. Melingui, O. Lakhal, B. Daachi, J. B. Mbede and R. Merzouki, "Adaptive Neural Network Control of a Compact Bionic Handling Arm," IEEE/ASME Transactions on Mechatronics, Vol.20, No.6, pp.2862-2875, Dec. 2015.

[21] G. Cai, J. Dias and L. Seneviratne, "A Survey of Small-Scale Unmanned Aerial Vehicles: Recent Advances and Future Development Trends," Unmanned Systems, Vol.2, No.2, pp.1-25, April 2014.

[22] J. Umenberger and A. H. Goktogan, "System identification and control of a small-scale paramotor," 2013 IEEE International Conference on Robotics and Automation (ICRA), Karlsruhe, Germany, May 2013, pp.2970-2976.

[23] M. Tanaka, H. Kawai, K. Tanaka and H. O. Wang, "Development of an autonomous flying robot and its verification via flight control experiment," 2013 IEEE International Conference on Robotics and Automation, Karlsruhe, Germany, May 2013, pp.4439-4444.

[24] T. M. Barrows, "Multibody Parafoil Model," 20th AIAA Aerodynamic Decelerator Systems Technology Conference and Seminar, Seattle, Washington, May 2009, AIAA 2009-2945.

[25] T. M. Barrows, "Apparent Mass of Parafoils with Spanwise Camber," Journal of Aircraft, vol.39, no.3, pp. 445-451, May-June 2002.

[26] K. Tanaka and H. O. Wang: Fuzzy Control Systems Design and Analysis: A Linear Matrix Inequality Approach, JOHN WILEY & SONS, INC, 2001

[27] K Tanaka, H Ohtake, H. O. Wang, "Guaranteed cost control of polynomial fuzzy systems via a sum of squares approach," IEEE Transactions on Systems, Man, and Cybernetics, Part B: Cybernetics, Vol.39, No.2, pp.561-567, April 2009.

[28] S. Boyd, et al., Linear Matrix Inequalities in System and Control Theory, volume 15 of Studies in Applied Mathematics, SIAM, Philadelphia, PA, June 1994.

[29] N. Sun, Y. Fang, H. Chen, B. Lu, "Amplitude-saturated nonlinear output feedback antiswing control for underactuated cranes with double-pendulum cargo dynamics," IEEE Transactions on Industrial Electronics, online published, DOI: 10.1109/TIE.2016.2623258.

[30] N. Sun, Y. Wu, Y. Fang, H. Chen, B. Lu, "Nonlinear continuous global stabilization control for underactuated RTAC systems: Design, analysis, and experimentation," IEEE/ASME Transactions on Mechatronics, online published, DOI: 10.1109/TMECH.2016.2631550.

[31] K. Tanaka, H. Ohtake and H. O. Wang, "A sum of squares approach to modeling and control of nonlinear dynamical systems with polynomial fuzzy systems," IEEE Transactions on Fuzzy Systems, Vol.17, No.4, pp.911-922, August 2009.